Scaling Effect in the Area-Averaged Fraction of Vegetation Cover Derived by Linear Mixture Model with Two-Band Spectral Vegetation Index Constraint

Kenta Obata [a] and Alfredo R. Huete [b]

[a]National Institute of Advanced Industrial Science and Technology,
Tsukuba, Ibaraki 305-8568, Japan
kenta_obata10@yahoo.co.jp (KO)
[b]University of Technology, Syedney, Plant Functional Biology and Climate Change Cluster,
Broadway NSW 2007, Australia
Alfredo.Huete@uts.edu.au (AH)

ABSTRACT

Multi-sensor analysis for monitoring terrestrial vegetation suffers from systematic errors due to the differences in spatial resolution, called scaling effect. This study investigates mechanisms underlying the scaling effect on fraction of vegetation cover (FVC) estimation, derived using a two-band spectral vegetation index (VI)-isoline based linear mixture model (VI-isoline based LMM). The two-band spectral VI includes a normalized difference vegetation index (NDVI), a soil-adjusted vegetation index (SAVI), and a two-band enhanced vegetation index (EVI2). A focus of this study is the monotonicity in an area-averaged FVC estimation along with spatial resolution. The proof of monotonicity provides intrinsic uncertainties (error bounds) of the area-averaged FVC attributed to scaling effect. A resolution transformation model was employed to investigate the monotonicity and derived results showed that a factor ξ, a function of 'true' and 'estimated' endmember spectra of vegetated and non-vegetated surfaces, is responsible for distinguishing the monotonicity and the non-monotonicity as well as increasing/decreasing trend of the area-averaged FVC along with spatial resolution. When the averaged FVC was monotonic, the increasing/decreasing trend was identical across FVCs derived using different two-band VIs. The derived results also described the condition by which scaling effect in the FVC is eliminated. Such findings were adverse to the scaling theory of two-band VI. Numerical experiments with a simulated spectral image verified the relationship between the monotonicity and the spectral conditions. The practicality of the scaling theory and the possibility of developing a scale-invariant FVC algorithm using two-band VI were evaluated in numerical experiments with Landsat7-ETM+ data.

Keywords: scaling effect, fraction of vegetation cover (FVC), two-band spectral vegetation index, resolution transformation model, linear mixture model (LMM)

1. INTRODUCTION

Remotely sensed data of the Earth surface is an important source of information with respect to dynamics in terrestrial vegetation, providing key measurements for climate, hydrologic, and biogeochemical studies.[1] A characteristics in the data is unique to temporal, spatial, and spectral resolutions of the satellite sensor that depends on the observation mission and technological advancement. The huge amount of earth observation data from multiple sensors are available[2] and data continuity and fusion studies are currently the challenges in remote sensing to take advantage those data for the accurate and continuous monitoring. Data continuity studies address to generate seamless, long-term data record to continuously and consistently monitor the earth surface.[3–5] Several studies examined the data continuity of biophysical retrievals, for example, the continuity of a normalized difference vegetation index (NDVI)[6] among Advanced Very High Resolution Radiometer (AVHRR) sensor series and Moderate Resolution Imaging Spectrometer (MODIS) onboard Terra and Aqua satellites,[5,7,8] in addition to Visible/Infrared Imager/Radiometer Suite (VIIRS) onboard the Suomi National Polar-orbiting Partnership (NPP).[9]

The differences in a sensor and a platform characteristics such as bandpass filter, a size of instantaneous field of view (IFOV), and sun-target-sensor viewing geometry generate systematic errors on biophysical retrievals derived using a reflectance spectrum. The differences would deteriorate the consistency among the satellite products from multiple sensors and it's increasingly important to mitigate the systematic errors for preserving the data continuity.[10]

An effect of the IFOV size, i.e., spatial resolution is one of major issues in a study of the biophysical retrievals.[11] It has been intensively discussed in geography and remote sensing research areas as the modifiable aerial unit problem (MAUP).[12] An interest of this study is systematic errors in an area-averaged values of biophysical retrievals over a fixed area, caused by differences in spatial resolution that is identical to a 'scale problem' in MAUP.[13–15] The systematic errors are referred as scaling effect in this study.[16] The scaling effect in biophysical retrievals would be typically larger as the spatial resolution decrease. The NDVI scaling effect has been investigated using theoretical techniques to identify intrinsic uncertainties of scaling effect (i.e., error bounds of scaling effect).[17–19]

Recent scaling studies investigated scaling effect of two-band vegetation index (two-band VI) as a function of spatial resolution under two-endmember linear mixture model (LMM),[16,20] by focusing on the monotonicity of the area-averaged two-band VI along with spatial resolution. The two-band VI is written by a rational function of two bands, i.e., red and near infrared (NIR) bands including NDVI, a soil adjusted vegetation index (SAVI),[21] and a two-band enhanced vegetation index (EVI2).[22] The area-averaged VI does not necessarily shift monotonically from coarser to finer resolution while it is monotonic under a certain resolution sequence that transforms spatial resolution from coarser to finer, called a resolution class.[20] The monotonicity in the resolution class underpinned the error bounds of scaling effect since the coarsest and finest resolutions (lumped and distributed cases[18]) in the resolution class are definitely either a minimum or a maximum of the averaged values. If it is non-monotonic, on the other hand, the error bounds cannot be identified.

Of particular interest in this study is the monotonicity of the fraction of vegetation cover (FVC) estimation as a function of spatial resolution. The FVC is one variable used to measure the horizontal spread of vegetation (a projected area of vegetation canopy over surface) and is defined as the ratio of the vegetated area to the entire pixel area in a satellite image.[23] The linear mixture model (LMM) is among one of the most frequently used methods to derive FVC in which a target spectrum is modeled by the linear sum of endmember spectra (pure spectra), involving a spectrum of vegetation canopy. In this study, the two-band vegetation index (VI)-isoline based LMM was selected to estimate FVC. It incorporates LMM with vegetation indices which takes the advantage of vegetation indices that is prone to mitigate unexpected influences associated with topographic effect (shadow effect), soil brightness, and aerosol contamination.

The monotonicity of the area-average FVC estimated using NDVI-isoline based LMM was thoroughly investigated using the resolution transformation model.[24] The study showed that the area-averaged NDVI-isoline based FVC is not necessarily monotonic within the resolution class, even though the area-averaged NDVI was a monotonic function of spatial resolution.[16] The monotonicity, non-monotonicity, and increasing/decreasing trend are specific to a factor ζ which is a function of spectral parameters of vegetation and non-vegetation over a target area and the model. The results also indicated the condition by which scaling effect of the area-averaged NDVI-isoline base FVC is eliminated. The previous scaling studies, however, have not investigated mechanisms underlying scaling effect of the FVC derived by a two-band VI-isoline based LMM.

The objective of this study is to investigates mechanisms underlying scaling effect on an area-averaged value of FVC estimation derived using two-band VI-isoline based LMM, base on the resolution transformation model under a two-endmember LMM. The monotonicity of the area-averaged isoline based FVC was investigated analytically and summarized into theorems. The theory derived in this study is validated and evaluated with spectral data simulated and measured by Enhanced Thematic Mapper Plus (ETM+) onboard Landsat7. Section 2 introduces the scaling effect on isoline based FVC. The analysis of the scaling effect is provided in Sec. 3. Section 4 validates and evaluates the scaling theory by numerical simulations of the simulated data and ETM+ data, followed by discussion and conclusion in Sec. 5 and 6, respectively.

2. SCALING EFFECT ON AREA-AVERAGED ISOLINE BASED FVC

Two-band VI, e.g., NDVI, SAVI, and EVI2 falls into a general form written as

$$v = \frac{p_1\rho_r + q_1\rho_n + r_1}{p_2\rho_r + q_2\rho_n + r_2}, \tag{1}$$

where ρ_r and ρ_n are red and NIR reflectances of the target, respectively and coefficients p_1, p_2, q_1, q_2, r_1, and r_2 are unique to a choice of the VI.[25]

A target spectrum is modeled by a linear mixture of vegetation and non-vegetation endmember spectra with red and NIR reflectances. The vegetation endmember spectrum assumed in the model is denoted by $\hat{\boldsymbol{\rho}}_v = (\hat{\rho}_{v,r}, \hat{\rho}_{v,n})$ and the non-vegetation endmember spectrum in the model is denoted by $\hat{\boldsymbol{\rho}}_s = (\hat{\rho}_{s,r}, \hat{\rho}_{s,n})$. The modeled spectrum is then written as

$$\hat{\boldsymbol{\rho}} = \hat{\omega}\hat{\boldsymbol{\rho}}_v + (1-\hat{\omega})\hat{\boldsymbol{\rho}}_s, \tag{2}$$

where $\hat{\omega}$ is a FVC estimation and $\hat{\boldsymbol{\rho}} = (\hat{\rho}_r, \hat{\rho}_n)$ is a modeled spectrum consists of red and NIR reflectances. The isoline based FVC is derived under the condition in which two-band VI calculated from the modeled and target spectra are identical,[26]

$$\hat{v}(\hat{\boldsymbol{\rho}}) = v(\boldsymbol{\rho}), \tag{3}$$

where $\boldsymbol{\rho} = (\rho_r, \rho_n)$, $\hat{v}$ and v are the modeled and target VIs. By solving for $\hat{\omega}$ which is implicitly included in $\hat{\boldsymbol{\rho}}$, an equation of the isoline based FVC can be obtained,

$$\hat{\omega} = \frac{(\boldsymbol{c}_1 - v\boldsymbol{c}_2)\cdot\hat{\boldsymbol{\rho}}_s + r_1 - vr_2}{(v\boldsymbol{c}_2 - c_1)\cdot(\hat{\boldsymbol{\rho}}_v - \hat{\boldsymbol{\rho}}_s)}, \tag{4}$$

where $\boldsymbol{c}_1 = (p_1, q_1)$, $\boldsymbol{c}_2 = (p_2, q_2)$.

The scaling effect of the isoline based FVC is simulated using Landsat7-ETM+ L1G data as the followings. A test site is west and suburbs of Sydney, Australia as shown in Fig. 1a. The data is a part of a scene of Landsat7-ETM+, path is 83 and row is 89, measured on December 1st, 2001. The size of data is 15.36 km by 15.36 km (512×512 pixels). The top-of-atmosphere reflectances were derived and atmospheric correction was not performed for this simulation. The data of 30m spatial resolution was aggregated into several resolutions, resulting in generating a set of coarser resolution elements C_0 where the number of pixel is written as

$$C_0 = \{1, 2^2, 4^2, 8^2, 16^2, 32^2, 64^2, 128^2, 256^2, 512^2\}. \tag{5}$$

Each resolution element in C_0 corresponds to the pixel size summarized in Tab. 1.

Table 1. Relationship between the number of pixel and the pixel size in the sample data.

Number of pixel	1	4	16	64	256	1,024	4,096	16,384	65,536	262,144
Size of pixel [m]	15,360	7,680	3,840	1,920	960	480	240	120	60	30

Two pairs of vegetation and non-vegetation endmembers in the model ($\hat{\boldsymbol{\rho}}_v$ and $\hat{\boldsymbol{\rho}}_s$), were prepared arbitrarily. The vegetation and non-vegetation endmember spectra for a first example (EM1) are (0.05,0.4) and (0.05,0.05), respectively. The endmember spectra for a second example (EM2) are (0.05,0.4) and (0.35,0.35). Area-averaged FVC, $\overline{\hat{\omega}}_j$($j$ is the number of pixel in Tab. 2) was computed for all the resolutions in C_0, from which the averaged FVC of the raw resolution (512^2 pixels), $\overline{\hat{\omega}}_N$ ($N = 512^2$), was subtracted, hence resultant values (residuals), $\Delta\overline{\hat{\omega}}_{j\to N}$, were the scaling effect (Eq. (6)). NDVI and EVI2 were selected as the condition to derive FVC estimation.

$$\Delta\overline{\hat{\omega}}_{j\to N} = \overline{\hat{\omega}}_j - \overline{\hat{\omega}}_N. \tag{6}$$

An example of the scaling effect on the averaged FVC derived using NDVI and EVI2 is shown in Fig. 1. The circle and square symbols correspond to EM1 and EM2, respectively. The solid and dashed lines are for NDVI and EVI2, respectively. The area-averaged FVC varies with spatial resolution and different trends (increasing and decreasing) are clearly seen in EM1 and EM2 although these are not necessarily monotonic (it will be discussed in Sec. 4 and 5.) The NDVI- and EVI2-isoline based FVC increase as the number of pixel increase when EM1 was selected in the LMM. On the other hand, the FVCs decrease when EM2 was selected. The magnitude of the scaling effect in the NDVI-isoline based FVC was greater than EVI2-isoline based FVC.

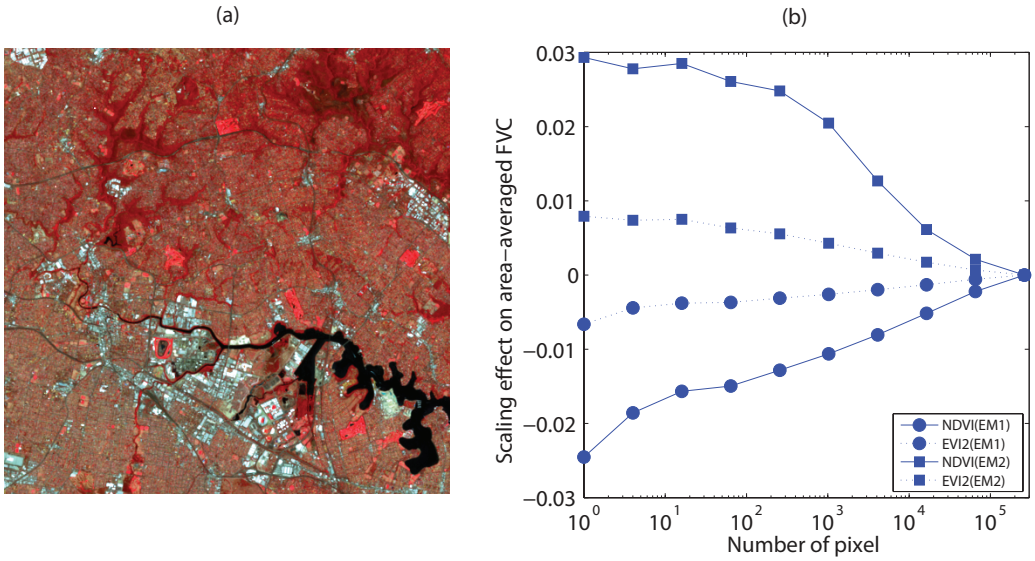

Figure 1. (a) A false color image of the test site measured by Landsat7-ETM+, west and suburbs of Sydney, Australia. (b) Scaling effect on the area-averaged isoline based FVC using NDVI and EVI2 as the condition along with spatial resolution (number of pixel) in the test site. Endmember spectra-1 (EM1) corresponds to increasing trend of the averaged FVC while endmember spectra-2 (EM2) corresponds to decreasing trend.

3. THEORETICAL ANALYSIS OF SCALING EFFECT ON THE FVC ESTIMATION

3.1 Derivation of a general form for isoline based FVC

To facilitate the analysis of the FVC scaling effect, a general form of the FVC estimation is derived in this section. Equation (1) is first linearly transformed and translated (Eq. (7)). The transformation and the translation are described in detail at the Appendix A. The two-band VI as a function of reflectances in a new coordinate, v^* is written by

$$v^* = \frac{\rho_n^* - \rho_r^*}{\rho_n^* + \mu\rho_r^*}, \tag{7}$$

where

$$\mu = -\frac{p_2 q_1}{p_1 q_2}, \tag{8}$$

where ρ_r^* and ρ_n^* are red and NIR reflectances in the new coordinate. A variable μ is dependent on the choice of two-band VI, for example, μ for NDVI, SAVI, and EVI2 are 1.0, 1.0, and 0.417.

The modeled reflectance in the new coordinate is written by

$$\hat{\boldsymbol{\rho}}^* = \hat{\omega}\hat{\boldsymbol{\rho}}_v^* + (1-\hat{\omega})\hat{\boldsymbol{\rho}}_s^*, \tag{9}$$

where $\hat{\boldsymbol{\rho}}^* = (\hat{\rho}_r^*, \hat{\rho}_n^*)$, $\hat{\boldsymbol{\rho}}_v^* = (\hat{\rho}_{v,r}^*, \hat{\rho}_{v,n}^*)$, and $\hat{\boldsymbol{\rho}}_s^* = (\hat{\rho}_{s,r}^*, \hat{\rho}_{s,n}^*)$.

The two-band VIs derived from the modeled and the target spectrum should be identical to derive FVC estimation,

$$\hat{v}^*(\hat{\boldsymbol{\rho}}^*) = v^*(\boldsymbol{\rho}^*), \tag{10}$$

where

$$\boldsymbol{\rho}^* = (\rho_r^*, \rho_n^*), \tag{11}$$
$$\hat{\boldsymbol{\rho}}^* = (\hat{\rho}_r^*, \hat{\rho}_n^*). \tag{12}$$

Eventually the FVC estimation is derived by solving for $\hat{\omega}$

$$\hat{\omega} = \frac{\hat{v}_s^* - v^*}{\hat{\eta}^*(v^* - \hat{v}_v^*) - v^* + \hat{v}_s^*}, \tag{13}$$

where a variable $\hat{\eta}$ is a ratio of L-1 norm of vegetation endmember to non-vegetation endmember.

$$v^* = \frac{\rho_n^* - \rho_r^*}{\rho_n^* + \mu\rho_r^*}, \tag{14a}$$
$$\hat{v}_v^* = \frac{\hat{\rho}_{v,n}^* - \hat{\rho}_{v,r}^*}{\hat{\rho}_{v,n}^* + \mu\hat{\rho}_{v,r}^*}, \tag{14b}$$
$$\hat{v}_s^* = \frac{\hat{\rho}_{s,n}^* - \hat{\rho}_{s,r}^*}{\hat{\rho}_{s,n}^* + \mu\hat{\rho}_{s,r}^*}, \tag{14c}$$
$$\hat{\eta}^* = \frac{\hat{\rho}_{v,n}^* + \mu\hat{\rho}_{v,r}^*}{\hat{\rho}_{s,n}^* + \mu\hat{\rho}_{s,r}^*}. \tag{14d}$$

The monotonicity of the area-averaged FVC is investigated using Eq. (13) in the following subsections.

3.2 Resolution Transformation Model

The target spectrum is also represented by a linear sum of a true vegetation and a true non-vegetation endmember spectra ($\boldsymbol{\rho}_v^*$ and $\boldsymbol{\rho}_s^*$) with a true value of FVC (ω) based on two-endmember LMM in an effort to analyze the scaling effect theoretically,

$$\boldsymbol{\rho}^* = \omega\boldsymbol{\rho}_v^* + (1-\omega)\boldsymbol{\rho}_s^*, \tag{15}$$

where

$$\boldsymbol{\rho}_v^* = (\rho_{v,r}^*, \rho_{v,n}^*), \tag{16}$$
$$\boldsymbol{\rho}_s^* = (\rho_{s,r}^*, \rho_{s,n}^*). \tag{17}$$

Note that this study defined an 'estimated' and a 'true' FVCs and the former is the target to be analyzed. The FVC estimation is rewritten by substituting Eq. (15) into Eq. (13),

$$\hat{\omega} = \frac{\det(\Delta\boldsymbol{\rho}^*, \hat{\boldsymbol{\rho}}_s^*)\omega + \det(\Delta\hat{\boldsymbol{\rho}}^*, \boldsymbol{\rho}_s^*)}{\det(\Delta\hat{\boldsymbol{\rho}}^*, \Delta\boldsymbol{\rho}^*)\omega + \det(\Delta\hat{\boldsymbol{\rho}}^*, \boldsymbol{\rho}_s^*)}, \tag{18}$$

where a term 'det' is a determinant of a 2-by-2 matrix consists of two vectors in the parenthesis, and

$$\Delta\boldsymbol{\rho}^* = (\Delta\rho_r^*, \Delta\rho_n^*), \tag{19a}$$
$$\Delta\hat{\boldsymbol{\rho}}^* = (\Delta\hat{\rho}_r^*, \Delta\hat{\rho}_n^*), \tag{19b}$$
$$\Delta\rho_r^* = \rho_{v,r}^* - \rho_{s,r}^*, \tag{19c}$$
$$\Delta\rho_n^* = \rho_{v,n}^* - \rho_{s,n}^*, \tag{19d}$$
$$\Delta\hat{\rho}_r^* = \hat{\rho}_{v,r}^* - \hat{\rho}_{s,r}^*, \tag{19e}$$
$$\Delta\hat{\rho}_n^* = \hat{\rho}_{v,n}^* - \hat{\rho}_{s,n}^*. \tag{19f}$$

In this study, spatial resolution is represented by the number of pixel, j, over a fixed area. A pixel in the image data is identified by k. The definition and illustration of the resolution transformation model for isoline based FVC estimation are introduced in Fig. 2. The FVC estimation for k-th pixel in j-th resolution is represented by

$$\hat{\omega}_{j,k} = \frac{\det(\Delta\boldsymbol{\rho}^*, \hat{\boldsymbol{\rho}}_s^*)\omega_{j,k} + \det(\Delta\hat{\boldsymbol{\rho}}^*, \boldsymbol{\rho}_s^*)}{\det(\Delta\hat{\boldsymbol{\rho}}^*, \Delta\boldsymbol{\rho}^*)\omega_{j,k} + \det(\Delta\hat{\boldsymbol{\rho}}^*, \boldsymbol{\rho}_s^*)}. \tag{20}$$

Area-averaged values of the FVC estimation for j-th resolution is written by

$$\overline{\hat{\omega}}_j = \sum_{k=1}^{j} \phi_{j,k}\hat{\omega}_{j,k}, \tag{21}$$

where $\phi_{j,k}$ is a fractional area of k-th pixel over a total area of j-th resolution data.

Scaling effect of isoline based FVC is analyzed using a minimum and a second minimum units of spatial resolutions. An interest of this study is therefore to analyze a difference between an FVC of 1st resolution and an area-averaged FVC of 2nd resolution ($\overline{\hat{\omega}}_2$ minus $\overline{\hat{\omega}}_1$),

$$\Delta\overline{\hat{\omega}} = \overline{\hat{\omega}}_2 - \overline{\hat{\omega}}_1. \tag{22}$$

The invariance in a sign of $\Delta\overline{\hat{\omega}}$ for every resolution transformation results in a monotonic behavior of the area-averaged FVC estimation. The reason is that spatial resolution is transformed by a repetition of dividing the pixel into two[16] and the scaling effect between area-averaged FVC of any two resolutions are a function of $\Delta\overline{\hat{\omega}}$'s generated in the series of resolution transformations.

A factor which varies in every resolution transformation is only $\omega_{2,1}$ (1st pixel in 2nd resolution) and $\phi_{2,1}$ as endmember spectra and ω_1 are constant and $\omega_{2,2}$ is a function of ω_1 and $\omega_{2,1}$ [$\omega_1 = \phi_{2,1}\omega_{2,1} + (1-\phi_{2,1})\omega_{2,2}$]. If a sign of $\Delta\overline{\hat{\omega}}$ would be invariant along with $\omega_{2,1}$ and $\phi_{2,1}$ (zero to unity) the area-averaged FVC will be monotonic. To analyze changes in the sign, a partial derivative of $\Delta\overline{\hat{\omega}}$ with respect to $\omega_{2,1}$ is investigated in the next subsection.

3.3 Analysis of a minimum unit of the scaling effect

The partiald derivative of $\Delta\overline{\hat{\omega}}$ with respect to $\omega_{2,1}$ was derived and analyzed in Appendix B. As a result, Eq. (23) were derived, representing the sign of $\Delta\overline{\hat{\omega}}$ is not always constant along with $\omega_{2,1}$. The sign (or a value) of $\Delta\overline{\hat{\omega}}$ depends only on a variable ξ, a function of the 'true' and the 'estimated' endmember spectra regardless of $\phi_{2,1}$ and the coefficient μ specific to the choice of two-band VI and true FVCs,

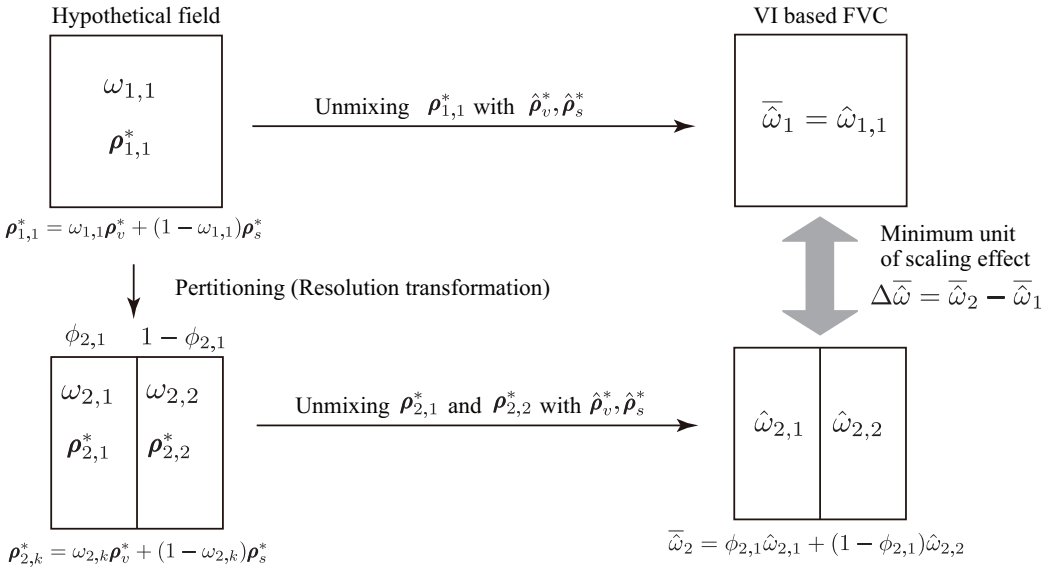

Figure 2. Illustration of resolution transformation model. The spatial resolution is transformed by partitioning a single pixel into two. The reflectance spectra are represented by linear mixture model (LMM) (left side of the figure), which are unmixed to estimate FVC (right side of the figure). The difference between the averaged FVC of 1st and 2nd resolution, $\Delta\overline{\hat{\omega}}$, is a key to analyze the monotonicity in the area-averaged FVC estimation.

$$\Delta\overline{\hat{\omega}} \begin{cases} \leq 0, & (\xi > 1), \\ = 0, & (\xi = 1), \\ \geq 0, & (0 \leq \xi < 1), \\ \text{the sign is variable}, & (\xi < 0), \end{cases} \tag{23}$$

where

$$\xi = \frac{\det(\Delta\hat{\boldsymbol{\rho}}^*, \boldsymbol{\rho}^*_s)}{\det(\Delta\hat{\boldsymbol{\rho}}^*, \boldsymbol{\rho}^*_v)}. \tag{24}$$

The sign of the $\Delta\overline{\hat{\omega}}$ is invariant if the value of ξ is equal to or higher than zero, whereas the sign is variable if the value of ξ is less than zero.

A condition $(\xi = 1)$ is identical to $[\det(\Delta\hat{\boldsymbol{\rho}}^*, \Delta\boldsymbol{\rho}^*) = 0]$ that indicates that the two vectors, differences between estimated vegetation and non-vegetation endmember spectra and between true vegetation and non-vegetation endmember spectra, $\Delta\hat{\boldsymbol{\rho}}^*$ and $\Delta\boldsymbol{\rho}^*$, are aligned in a parallel manner in the transformed and translated red and NIR reflectance space (Fig. 3). Since endmember variables here are linearly converted from the original coordinate, the condition, $(\xi = 1)$, is identical across two-band VIs. It means that decreasing and increasing trends should be the same across FVCs derived using any two-band VI. Remind that the area-averaged FVC estimation should be scale invariant when either $(\omega_{2,1} = \omega_{2,2})$ or $[\det(\Delta\hat{\boldsymbol{\rho}}^*, \Delta\boldsymbol{\rho}^*) = 0]$ is satisfied.

3.4 Monotonicity of the Area-averaged FVC

A set of resolution elements created with the repetition of resolution transformation is called 'resolution class'[16] modeling consecutive changes in spatial resolution from coarser to finer resolution. We summarized the derived results into theorems with regard to the monotonicity in the area-averaged FVC.

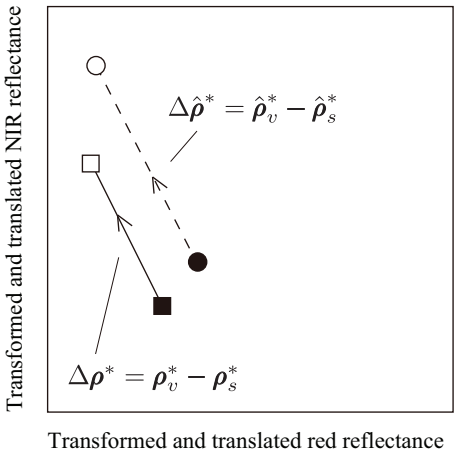

Figure 3. Illustration of the parallel relationship between the two vectors described by the true endmember spectra and the assumed endmember spectra over the transformed and translated coordinate ($\Delta\hat{\boldsymbol{\rho}}^*$ and $\Delta\boldsymbol{\rho}^*$). Empty and filled squares indicate the vegetation and non-vegetation endmember spectra in the hypothetical field, and empty and filled circles indicate the assumed endmember spectra in the LMM. When the two vectors are parallel, scaling effects are not observed in the averaged isoline based FVC.

THEOREM 3.1. Under a single resolution class, the area-averaged isoline based FVC values change monotonically as a function of the spatial resolution if $\xi \geq 0$.

When this is the case,

THEOREM 3.2. The area-averaged FVC values follow a trend determined by ξ such that estimation of the averaged isoline based FVC is a non-increasing function if $\xi > 1$, whereas it is a non-decreasing function if $\xi \geq 0$.

On the one hand, the average FVC can change non-monotonically for $\xi < 0$ because the relationship between the average FVC values determined at two resolutions will vary.

4. NUMERICAL SIMULATION

4.1 Validation with simulated data

The monotonicity and the increasing/decreasing trend of the area-averaged FVC, i.e., Theorem 3.1 and 3.2, were verified with numerical simulations. A sample data and model inputs were prepared to satisfy the condition for the monotonic behavior in the area-averaged FVC ($\xi \geq 0$). A hypothetical field was simulated with a uniform vegetation and non-vegetation surfaces as shown in Fig. 5, which is the same data to that used in the study for two-band VI scaling effect[24] where its monotonicity was demonstrated numerically.

The number of pixel in finest resolution is 200^2 and all the pixels in the image are homogeneous, either vegetation or non-vegetation. The red and NIR reflectances for a vegetation spectrum are (0.05,0.4); and for a non-vegetation are (0.18,0.18).[24] The spectral data of the raw resolution is aggregated by arithmetic averaging to simulate coarser resolutions. Two examples of the resolution class, represented by the sets C_1 and C_2, were subsets of a set A_{40000} as

$$C_1 = \{1, 4, 16, 64, 1600, 40000\}, \tag{25}$$

$$C_2 = \{1, 25, 625, 2500, 10000, 40000\}, \tag{26}$$

where

$$A_{40000} = \{1, 4, 16, 25, 64, 100, 400, 625, 1600, 2500, 10000, 40000\}. \tag{27}$$

The set of resolution elements in A_{40000} was selected based on a manner for simulating an square image with square pixels and C_1 and C_1 follow the condition of the resolution class as described in previous study.[16]

To compute isoline based FVC estimation, NDVI, SAVI, and EVI2 were selected as the condition in the FVC algorithm. The endmember spectrum for vegetation assumed in the FVC algorithm was (0.04,0.35). Two sets of non-vegetation endmember spectra were defined, one was (0.05,0.05) and another was (0.2,0.2), denoted as EM3 and EM4, respectively. For every pixel in each resolution, isoline based FVC were derived and area-averaged FVC was computed on each resolution. The value of ξ identifying either monotonic increasing or decreasing is also computed for EM3 and EM4, which was (0.60, 0.83, 0.85) for NDVI, SAVI, and EVI2 on EM3, and was (1.25, 1.11, 1.10) for the three VIs on EM4. The use of EM3 expects non-increasing function while use of EM4 expects non-decreasing function.

Results of the simulation for EM3 are shown in Fig. 5. The area-averaged FVCs derived using NDVI, SAVI, and EVI2 change non-monotonically under the resolution sequence A_{40000} (Fig. 5a, d, and g) because of involving two variations of resolution class (C_1 and C_2). In the middle column of Fig. 5 (b, e, and h), the averaged FVCs of the set C_1 were connected with a solid line, showing monotonic increasing of the FVC along with spatial resolution. Similarly the averaged FVC of the set C_2 was a non-decreasing function in the rightmost column of Fig. 5 (c, f, and i). This increasing trend was identical among the three VIs that is also described in the theory we derived.

Results of the simulation for EM4 are shown in Fig. 6. The averaged FVC was also non-monotonic function in the sequence A_{40000} (Fig. 6a, d, and g), while it was monotonically shifted in the sequences C_1 (Fig. 6b, e, and h) and C_2 (Fig. 6c, f, and i). In each resolution class, the averaged FVC functioned as a monotonic non-decreasing parameter.

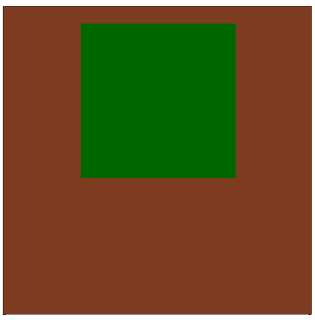

Figure 4. Hypothetical image of the target area[24] consisting of a uniform vegetation and a non-vegetation surfaces. The red and NIR reflectances for a vegetation spectrum are (0.05,0.4); and for a non-vegetation are (0.1,0.1), respectively.

4.2 Evaluation with Landsat7-ETM+ data

The theory of the scaling effect on area-averaged FVC was evaluated using Landsat7 ETM+ data. In a single pixel, however, there would be more than two endmember spectra (e.g., canopy, branch, shade, soil, artificial object, water, etc.), thus the theory is not exactly applicable in actual satellite data. The true endmember spectra are not available in the satellite data as well. Even though there is such a gap between the theory and actual data, we can evaluate the feasibility and possibility of the theory with actual data according to exploring 1) whether the trends in area-averaged isoline based FVC estimation (increasing and decreasing) change along with changes in endmember spectra in the FVC algorithm; and 2) whether the increasing and decreasing trends are the same across VIs used as the condition in the algorithm; and 3) whether there exists a set of endmember spectra minimizing/reducing the scaling effect of isoline based FVC that implicitly corresponds to the condition ($\xi = 1$).

The test site is identical to the image used in Sec. 2. The vegetation endmember in the FVC algorithm was (0.05,0.4). Several spectra of non-vegetation endmember were prepared in the simulation. The spectra were over the same soil line whose slope and offset were unity and zero. The red reflectance of the non-vegetation class was

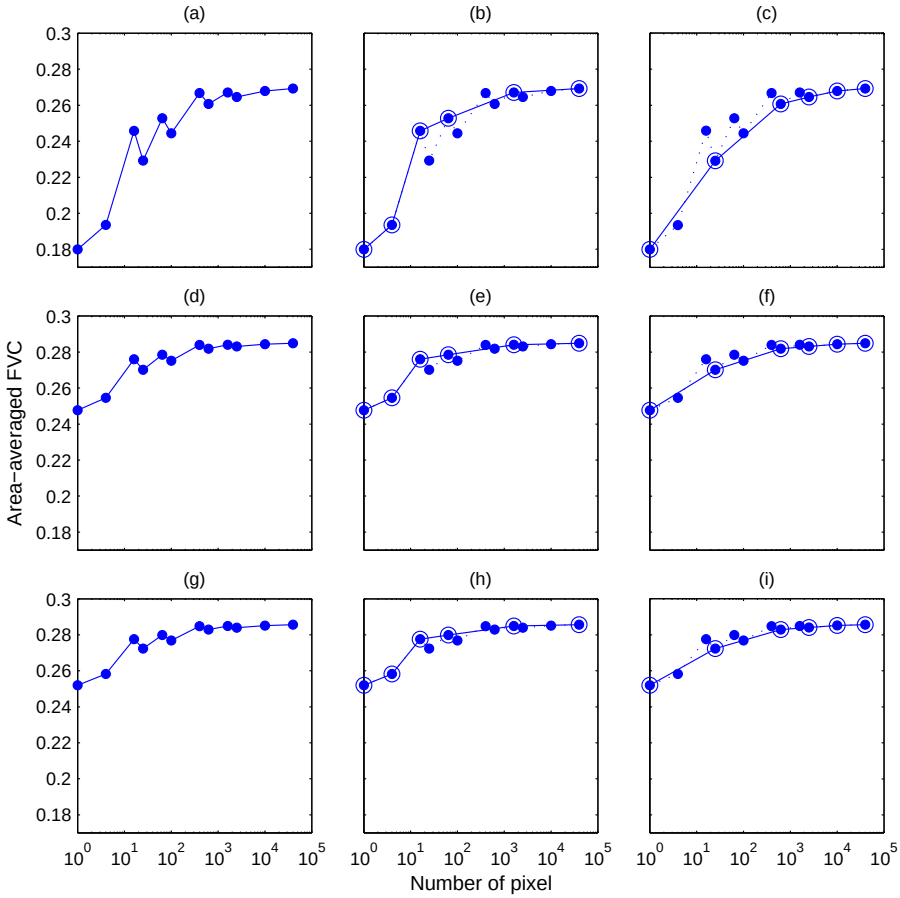

Figure 5. Area-averaged values of isoline based FVC as a function of the number of pixel for EM3 [vegetation endmember is (0.04,0.35), and non-vegetation endmember is (0.05,0.05).] An upper row, a middle row, and a lower row plot the averaged FVC derived using NDVI, SAVI, and EVI2, respectively. In a left column, the averaged FVC is computed for the resolution sequence, A_{40000}, and a middle and a right columns are for the sequences C_1 and C_2, respectively.

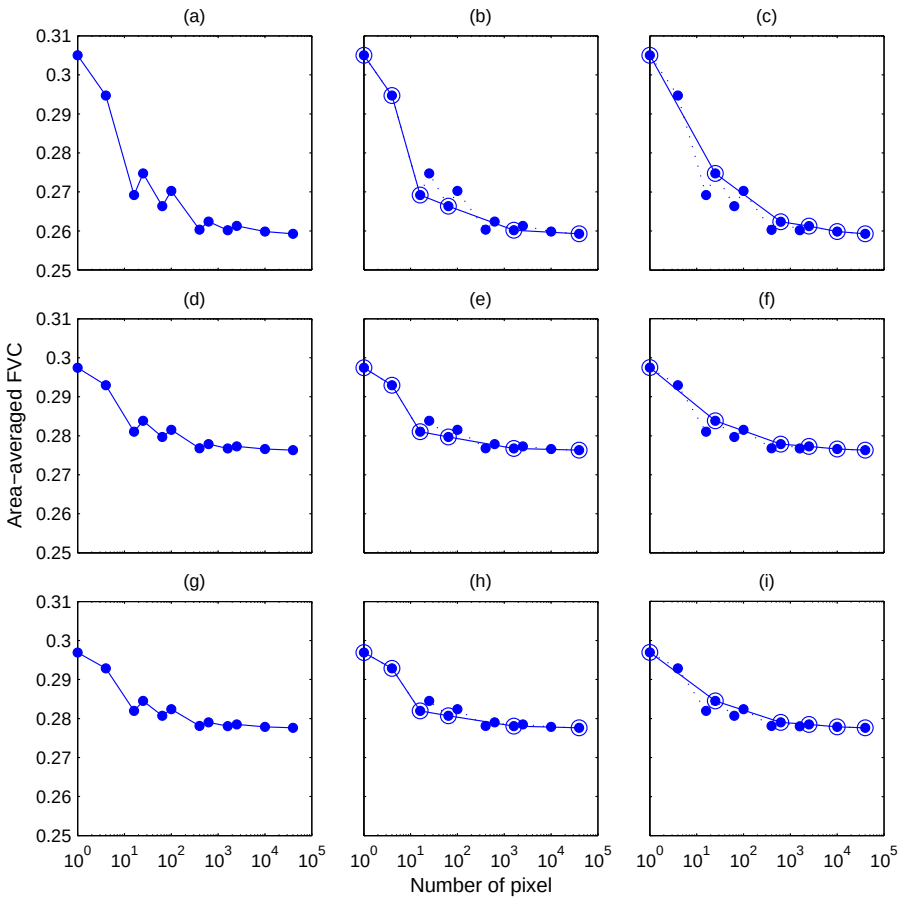

Figure 6. Area-averaged values of isoline based FVC as a function of the number of pixel for EM4 [vegetation endmember is (0.04,0.35), and non-vegetation endmember is (0.2,0.2).]

changed from 0.05 to 0.35 with 0.05 increment. Changes in the non-vegetation endmember implicitly indicated the value of ξ might have changed although the true endmeber spectra were unknown. The scaling effect of the area-averaged FVC was computed by applying Eq. (6) where $N = 200^2$ here.

Results of the simulation is shown in Fig. 7a, b, and c for the scaling effect of the averaged NDVI-, SAVI-, and EVI2-isoline based FVC as a function of spatial resolution. The magnitude of the scaling effect was larger in NDVI-isoline based FVC compared with SAVI and EVI2 ones. As the value of non-vegetation endmember increases, the magnitude and the sign of the scaling effect shift. For instance, NDVI-isoline based FVC scaling effect gradually increased with increasing red non-vegetation reflectance and the sign changed from negative to positive.

The scaling effect for lower red reflectances of non-vegetation endmember (0.05, 0.10, and 0.15) was basically negative whereas that for higher red reflectances (0.25, 0.30, and 0.35) was positive for the three VIs. The trend of increasing and decreasing tended to be identical across the two-band VIs.

The behavior in the filled diamond symbols in the Fig. 7a, b, and c represent that the averaged FVC derived by the three VIs were comparably close to zero when red the reflectance of non-vegetation endmember was 0.2. One could find the pair of endmember spectra which minimized/reduced scaling effect for the three VIs. When this is the case, a value of ξ for this simulation might have been close to unity, computed by endmember spectra in the FVC algorithm and actual data although there would be more than two endmember spectra. The result indicates the possibility of developing the scale-invariant FVC algorithm using two-band VI.

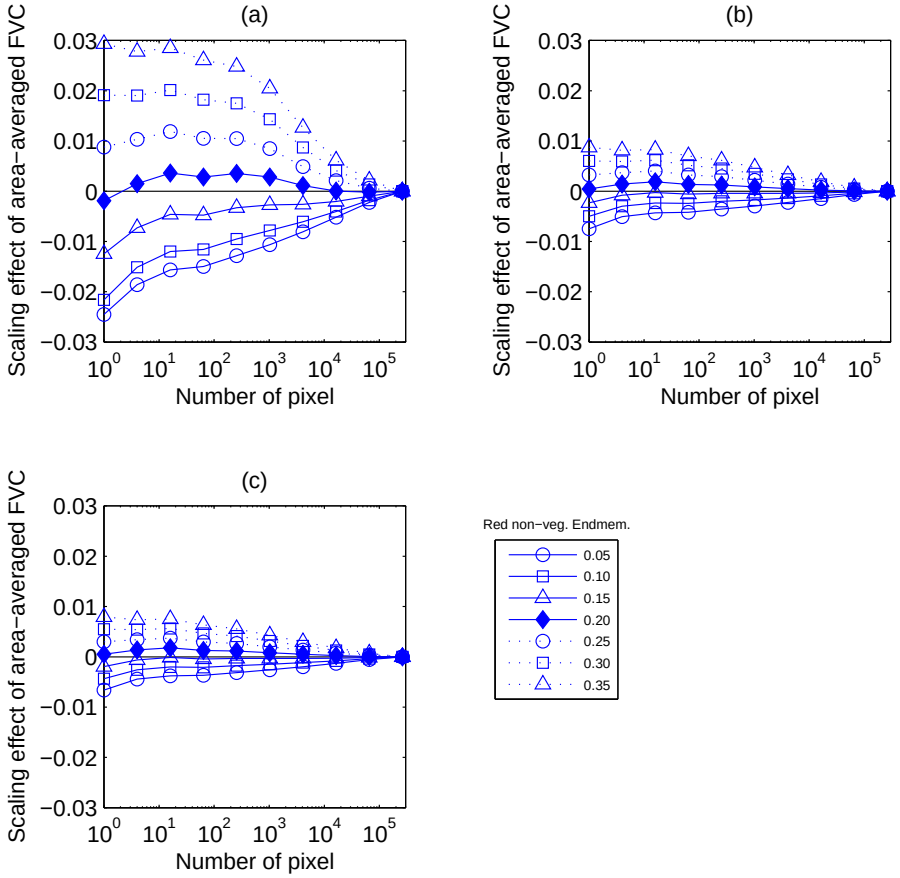

Figure 7. Scaling effect on area-averaged values of the isoline based FVC as a function of the number of pixel with Landsat7-ETM+ data. (a), (b), and (c) corresponds to results derived using NDVI, SAVI, and EVI2, respectively. Changes in the red reflectance of non-vegetation endmember spectrum in the FVC algorithm is shown at a legend box (0.05 to 0.35 with 0.05 increment).

5. DISCUSSION

The scaling effect underlying two-band VI including NDVI, SAVI, and EVI2 were investigated analytically in a previous study[20] where the monotonicity of the area-averaged two-band VI was demonstrated and a factor η_k identifying monotonic increasing and decreasing was found, which is a function of endmember spectra of the target spectrum and a coefficient $\nu = -(p_2q_1)/(p_1q_2)$ that depends on the choice of two-band VI. The derived results of the scaling effect and numerical simulations showed that the trend of increasing or decreasing along with spatial resolution was different among VIs. For example, in the residential area sparsely covered by small forest and trees, NDVI and SAVI increase along with spatial resolution but EVI2 was decreasing function.[20]

On contrary, this study demonstrated the facts that scaling effect underlying FVC estimation derived using two-band VI are totally different from the two-band VI scaling effect: 1) scaling effect underlying the area-averaged isoline based FVC estimation was not necessarily changed monotonically in a resolution class, and 2) the factor ξ, identifying the monotonicity and the trends does not have a coefficient which is characterized by the choice of two-band VI (μ), implying that trends of monotonic increasing and decreasing were identical for any choice of two-band VI as the condition in the isoline based FVC algorithm, and 3) the isoline based FVC has variables to be estimated (endmember spectra of vegetation and non-vegetation) and certain pairs of the endmember spectra reduce/minimize the scaling effect on the averaged FVC.

Series of scaling studies[16,20,24] and this study assumed the limited conditions for modeling scaling effect. We used 'two-endmember' LMM, only describing homogeneous vegetation and non-vegetation surfaces. The scaling effect of the area-averaged isoline-based FVC under the multiple-endmember assumption should be investigated by expanding the resolution transfer model. To analyze scaling effect theoretically, we also assumed the perfect sensor regarding a point spread function (PSF). The PSF in this study should be a rectangular rather than the Gaussian/triangle shape to characterize scaling effect analytically.

6. CONCLUSION

The scaling effect underlying an area-averaged fraction of vegetation cover (FVC) derived by two-band vegetation index (VI)-isoline based linear mixture model (VI-isoline based LMM) was investigated analytically based on a resolution transformation model. The monotonicity in the area-averaged FVC estimation along with spatial resolution was identified only if a value of ξ is equal or larger than zero, which is a function of true and estimated endmember spectra of vegetation and non-vegetation in the transformed and translated coordinate. If ξ is lower than zero, the area-averaged FVC is possible to be non-linear along with spatial resolution. The derived results were summarized into theorems. It was interesting that a value ξ is independent of μ that depends on the choice of two-band VI so that the condition distinguishing increasing and decreasing trends is identical among any choices of two-band VI in the FVC algorithm. The condition which eliminates scaling effect in the FVC was derived that indicates that the two vectors associated with endmember spectra of the target and the model were described in parallel manner over the reflectance space.

The monotonic behavior in the area-averaged VI-isoline based FVC was demonstrated by the simulated spectral data. The feasibility and possibility of the scaling theory was evaluated using Landsat7-ETM+ data. In general, the results obtained in the experiments agreed with the theory. However, a gap between actual data and the theory still exist because of the differences between the number of endmember spectra in actual data and the model.

Findings in this study supports to strengthen understandings in the theory of scaling effect underlying biophysical retrievals in the context of data continuity study. The condition for scale-invariance found in the FVC scaling theory should contribute to develop scale-invariant FVC estimation algorithm with two-band VI as the condition using multi-resolution satellite data set.

Acknowledgements

This work was supported by ... We would like to thank Dr. Hiroki Yoshioka for his advice and assistance on this work.

APPENDIX A. TRANSFORMATION AND TRANSLATION OF A GENERAL FORM

The procedure of deriving a general form of the two-band VI is introduced as explained in previous study.[24] The two-band VI, v, may be rewritten as

$$v = p_3 v', \tag{28}$$

where

$$v' = \frac{\rho_n + q_3\rho_r + r_3}{\rho_n + q_4\rho_r + r_4}, \tag{29}$$

and where $p_3 = q_1/q_2$, $q_3 = p_1/q_1$, $q_4 = p_2/q_2$, $r_3 = r_1/q_1$, and $r_4 = r_2/q_2$ are defined. Then reflectance spectrum over the red and NIR reflectance space (a vector space V over a field F), $\boldsymbol{\rho} \in V$, can be linearly transformed into $\boldsymbol{\rho}' \in W$ by a map $f: V \to W$,

$$\boldsymbol{\rho}' = f(\boldsymbol{\rho}) = \boldsymbol{T}\boldsymbol{\rho}, \tag{30}$$

where

$$\boldsymbol{T} = \begin{bmatrix} -q_3 & 0 \\ 0 & 1 \end{bmatrix}. \tag{31}$$

The value of the VI in Equation (29) can be expressed as a function of $\boldsymbol{\rho}'$, with $q_5 = -q_4/q_3$, as

$$v' = \frac{\rho'_n - \rho'_r + r_3}{\rho'_n + q_5\rho'_r + r_4}. \tag{32}$$

The spectrum $\boldsymbol{\rho}' \in W$ is then translated into $\boldsymbol{\rho}'' \in W$ by adding a vector $\boldsymbol{d}_1$

$$\boldsymbol{\rho}'' = \boldsymbol{\rho}' + \boldsymbol{d}_1, \tag{33}$$

where $\boldsymbol{d}_1$ is

$$\boldsymbol{d}_1 = \frac{r3}{2}\begin{bmatrix} -1 \\ 1 \end{bmatrix}. \tag{34}$$

Equation (32) can be represented in terms of $\boldsymbol{\rho}''$ according to

$$v' = \frac{\rho''_n - \rho''_r}{\rho''_n + q_5\rho''_r + r_5}, \tag{35}$$

where r_5 is defined by

$$r_5 = r_4 + \frac{q_5 - 1}{2} r_3. \tag{36}$$

Again, the spectrum $\boldsymbol{\rho}'' \in W$ can be translated into $\boldsymbol{\rho}''' \in W$ by adding a vector $\boldsymbol{d}_2$

$$\boldsymbol{\rho}''' = \boldsymbol{\rho}'' + \boldsymbol{d}_2, \tag{37}$$

where $\boldsymbol{d}_2$ is defined by

$$\boldsymbol{d}_2 = \frac{r_5}{1 + q_5}\begin{bmatrix} 1 \\ 1 \end{bmatrix}. \tag{38}$$

The final form of the transformed equations for a two-band VI becomes

$$v' = \frac{\rho'''_n - \rho'''_r}{\rho'''_n + q_5\rho'''_r}. \tag{39}$$

The coordinate system for the transformed space consists of $\boldsymbol{\rho}''' = (\rho_r''', \rho_n''')$ and can be restored back to the original coordinates ($\boldsymbol{\rho} = (\rho_r, \rho_n)$) by applying the inverse mapping $f^{-1}: W \rightarrow V$, after subtracting $\boldsymbol{d}_1$ and $\boldsymbol{d}_2$ from $\boldsymbol{\rho}'''$,

$$\boldsymbol{\rho} = f^{-1}(\boldsymbol{\rho}''' - \boldsymbol{d}_1 - \boldsymbol{d}_2) = \boldsymbol{T}^{-1}(\boldsymbol{\rho}''' - \boldsymbol{d}_1 - \boldsymbol{d}_2). \tag{40}$$

In Sec. 3 of this paper, Eq. (39) is represented as the following

$$v^* = \frac{\rho_n^* - \rho_r^*}{\rho_n^* + \mu\rho_r^*},$$

where v^*, μ, ρ_r^*, and ρ_n^* correspond to v', q_5, ρ_r''', and ρ_n'''.

APPENDIX B. PARTIAL DERIVATIVE OF A MINIMUM UNIT FOR DESCRIBING THE SCALING EFFECT

An analysis of the partial derivative of $\Delta\hat{\omega}$ with respect to $\omega_{2,1}$ is described here. The variable $\phi_{2,1}$ is a fraction of area of 1st pixel over a total area of 2nd resolution.

$$\frac{\partial\Delta\hat{\omega}}{\partial\omega_{2,1}} = \phi_{2,1}\frac{\partial\hat{\omega}_{2,1}}{\partial\omega_{2,1}} + (1-\phi_{2,1})\frac{\partial\hat{\omega}_{2,2}}{\partial\omega_{2,1}}. \tag{41}$$

A partial derivative of $\hat{\omega}_{2,1}$ with respect to $\omega_{2,1}$ is written by

$$\frac{\partial\hat{\omega}_{2,1}}{\partial\omega_{2,1}} = \frac{\det(\boldsymbol{\rho}_v^*, \boldsymbol{\rho}_s^*)\cdot\det(\hat{\boldsymbol{\rho}}_v^*, \hat{\boldsymbol{\rho}}_s^*)}{[\det(\Delta\hat{\boldsymbol{\rho}}^*, \Delta\boldsymbol{\rho}^*)\omega_{2,1} + \det(\Delta\hat{\boldsymbol{\rho}}^*, \boldsymbol{\rho}_s^*)]^2}. \tag{42}$$

Likewise, a partial derivative of $\hat{\omega}_{2,1}$ with respect to $\omega_{2,2}$ is written by

$$\frac{\partial\hat{\omega}_{2,2}}{\partial\omega_{2,1}} = \frac{\phi_{2,1}\det(\boldsymbol{\rho}_v^*, \boldsymbol{\rho}_s^*)\cdot\det(\hat{\boldsymbol{\rho}}_v^*, \hat{\boldsymbol{\rho}}_s^*)}{(\phi_{2,1}-1)[\det(\Delta\hat{\boldsymbol{\rho}}^*, \Delta\boldsymbol{\rho}^*)\omega_{2,1} + \det(\Delta\hat{\boldsymbol{\rho}}^*, \boldsymbol{\rho}_s^*)]^2}. \tag{43}$$

Equations (42) and (43) are substituted into Eq. (41), then it is written as

$$\frac{\partial\Delta\hat{\omega}}{\partial\omega_{2,1}} = \frac{\phi_{2,1}\det(\boldsymbol{\rho}_v^*, \boldsymbol{\rho}_s^*)\cdot\det(\hat{\boldsymbol{\rho}}_v^*, \hat{\boldsymbol{\rho}}_s^*)}{S_1^2 S_2^2}(S_2^2 - S_1^2), \tag{44}$$

where S_m $(m = 1, 2)$ is given as

$$S_m = \det(\Delta\hat{\boldsymbol{\rho}}^*, \Delta\boldsymbol{\rho}^*)\omega_{2,m} + \det(\Delta\hat{\boldsymbol{\rho}}^*, \boldsymbol{\rho}_s^*). \tag{45}$$

Two terms in Eq. (44), $[\det(\boldsymbol{\rho}_v^*, \boldsymbol{\rho}_s^*)]$ and $[\det(\hat{\boldsymbol{\rho}}_v^*, \hat{\boldsymbol{\rho}}_s^*)]$ are basically positive, because they can be rewritten as

$$\det(\boldsymbol{\rho}_v^*, \boldsymbol{\rho}_s^*) = \rho_{v,n}^*\rho_{s,n}^*(1+\mu)\left(\frac{\rho_{v,r}^*}{\rho_{v,n}^*} - \frac{\rho_{s,r}^*}{\rho_{s,n}^*}\right), \tag{46}$$

$$\det(\hat{\boldsymbol{\rho}}_v^*, \hat{\boldsymbol{\rho}}_s^*) = \hat{\rho}_{v,n}^*\hat{\rho}_{s,n}^*(1+\mu)\left(\frac{\hat{\rho}_{v,r}^*}{\hat{\rho}_{v,n}^*} - \frac{\hat{\rho}_{s,r}^*}{\hat{\rho}_{s,n}^*}\right), \tag{47}$$

where last parenthesis in Eqs. (46 and 47) are the same to the Ratio Vegetation Index (RVI) of (a true or an estimated) vegetation spectrum minus non-vegetation spectrum.[6]

The sign of the partial derivative relies on a term $(S_2^2 - S_1^2)$, which is also rewritten by

$$S_2^2 - S_1^2 = 2[\det(\Delta\hat{\boldsymbol{\rho}}^*, \Delta\boldsymbol{\rho}^*)]^2(\omega_{2,2} - \omega_{2,1})\left(\frac{\omega_{2,1} + \omega_{2,2}}{2} + \frac{1}{1-\xi}\right), \tag{48}$$

where

$$\xi = \frac{\det(\Delta\hat{\boldsymbol{\rho}}^*, \boldsymbol{\rho}_s^*)}{\det(\Delta\hat{\boldsymbol{\rho}}^*, \boldsymbol{\rho}_v^*)}. \tag{49}$$

Consequently the sign of the partial derivative varied with the value of ξ,

$$\text{If } \xi > 1, \qquad \frac{\partial \Delta\overline{\widehat{\omega}}}{\partial \omega_{2,1}} \begin{cases} > 0 & (\omega_{2,1} < \omega_{2,2}), \\ = 0 & (\omega_{2,1} = \omega_{2,2}), \\ < 0 & (\omega_{2,1} > \omega_{2,2}). \end{cases} \tag{50}$$

$$\text{If } 0 \le \xi < 1, \qquad \frac{\partial \Delta\overline{\widehat{\omega}}}{\partial \omega_{2,1}} \begin{cases} < 0 & (\omega_{2,1} < \omega_{2,2}), \\ = 0 & (\omega_{2,1} = \omega_{2,2}), \\ > 0 & (\omega_{2,1} > \omega_{2,2}). \end{cases} \tag{51}$$

The sign of $\partial\Delta\overline{\widehat{\omega}}/\partial\omega_{2,1}$ for $\xi < 0$, however, does not change monotonically with $\omega_{2,1}$.

REFERENCES

1. A. Huete, K. Didan, W. van Leeuwen andTomoaki Miura, and E. Glenn, "MODIS vegetation inidces," in *Land Remote Sensing and Global Environmental Change*, B. Ramachandran, C. O. Justice, and M. J. Abrams, eds., pp. 579–602, Springer, 2011.
2. G. Gutman and J. G. Masek, "Long-term time series of the Earth's land-surface observations from space," *Int. J. Remote Sens.* **33**(15), pp. 4700–4719, 2012.
3. M. Brown, J. Pinzon, K. Didan, J. Morisette, and C. Tucker, "Evaluation of the consistency of long-term NDVI time series derived from AVHRR,SPOT-vegetation, SeaWiFS, MODIS, and Landsat ETM+ sensors," *IEEE Trans. Geosci. Remote Sens.* **44**(7), pp. 1787 –1793, 2006.
4. R. Bryant, M. Moran, S. McElroy, C. Holifield, K. Thome, T. Miura, and S. Biggar, "Data continuity of Earth Observing 1 (EO-1) Advanced Land I satellite imager (ALI) and Landsat TM and ETM+," *IEEE Trans. Geosci. Remote Sens.* **41**(6), pp. 1204–1214, 2003.
5. R. Fensholt and S. R. Proud, "Evaluation of earth observation based global long term vegetation trends - comparing GIMMS and MODIS global NDVI time series," *Remote Sens. Environ.* **119**(0), pp. 131 – 147, 2012.
6. C. J. Tucker, "Red and photographic infrared linear combinations for monitoring vegetation," *Remote Sens. Environ.* **8**, pp. 127–150, 1979.
7. C. J. Tucker, J. E. Pinzon, M. E. Brown, D. A. Slayback, E. W. Pak, R. Mahoney, E. F. Vermote, and N. E. Saleous, "An extended AVHRR 8-km NDVI dataset compatible with MODIS and SPOT vegetation NDVI data," *Int. J. Remote Sens.* **26**(20), pp. 4485–4498, 2005.
8. L. Ji, K. Gallo, J. C. Eidenshink, and J. Dwyer, "Agreement evaluation of AVHRR and MODIS 16d-ay composite NDVI data sets," *Int. J. Remote Sens.* **29**(16), pp. 4839–4861, 2008.
9. T. Miura, J. Turner, and A. Huete, "Spectral compatibility of the NDVI across VIIRS, MODIS, and AVHRR: An analysis of atmospheric effects using EO-1 Hyperion," *Geoscience and Remote Sensing, IEEE Transactions on* **51**(3), pp. 1349–1359, 2013.
10. J. T. Overpeck, G. A. Meehl, S. Bony, and D. R. Easterling, "Climate data challenges in the 21st century," *Science* **331**(6018), pp. 700–702, 2011.
11. H. Wu and Z.-L. Li, "Scale issues in remote sensing: a review on analysis, processing and modeling," *Sensors* **9**, pp. 1768–1793, 2009.
12. S. Openshaw, *The Modifiable Areal Unit Problem*, Geo Books, Norwich, UK, 1984.
13. D. A. Quattrochi and M. F. Goodchild, *Scale in Remote Sensing and GIS*, Lewis Publishers, 1997.
14. D. J. Marceau and G. J. Hay, "Remote sensing contributions to the scale issue," *Can. J. Remote Sens.* **25**(4), pp. 357–366, 1999.

15. P. M. Atkinson and N. J. Tate, "Spatial scale problems and geostatistical solutions: A review," *Prof. Geogr.* **52**(4), pp. 607–623, 2000.
16. K. Obata, T. Wada, T. Miura, and H. Yoshioka, "Scaling effect of area-averaged NDVI: Monotonicity along the spatial resolution," *Remote Sens.* **4**(1), pp. 160–179, 2012.
17. M. Raffy, "Change of scale in models of remote sensing: A general method for spatialization of models," *Remote Sens. Environ.* **40**(2), pp. 101 – 112, 1992.
18. Z. Hu and S. Islam, "A frame work for analyzing and designing scale invariant remote sensing algorithms," *IEEE Trans. Geosci. Remote Sens.* **35**(3), pp. 747–755, 1997.
19. Z. Jiang, A. R. Huete, J. Chen, Y. Chen, J. Li, G. Yan, and X. Zhang, "Analysis of NDVI and scaled difference vegetation index retrievals of vegetation fraction," *Remote Sens. Environ.* **101**, pp. 366–378, 2006.
20. K. Obata, T. Miura, and H. Yoshioka, "Scaling effects in area-averaged values of two-band spectral vegetation indices represented in a general form," *J. Appl. Remote Sens.* **6**(1), pp. 063585–063585, 2012.
21. A. R. Huete, "A soil-adjusted vegetation index (SAVI)," *Remote Sens. Environ.* **25**(3), pp. 295 – 309, 1988.
22. Z. Jiang, A. R. Huete, K. Didan, and T. Miura, "Development of a two-band enhanced vegetation index without a blue band," *Remote Sens. Environ.* **112**(10), pp. 3833 – 3845, 2008.
23. M. O. Smith, P. E. Johnson, and J. B. Adams, "Quantitative determination of mineral types and abundances from reflectance spectra using principal components analysis," *J. Geophys. Res., Suppl.* **90**, pp. C797–C804, 1985.
24. K. Obata, T. Miura, and H. Yoshioka, "Analysis of the scaling effects in the area-averaged fraction of vegetation cover retrieved using an ndvi-isoline-based linear mixture model," *Remote Sens.* **4**(7), pp. 2156–2180, 2012.
25. K. Obata and H. Yoshioka, "Inter-algorithm relationships for the estimation of the fraction of vegetation cover based on a two endmember linear mixture model with the VI constraint," *Remote Sens.* **2**(7), pp. 1680–1701, 2010.
26. X. Zeng, R. E. Dickinson, A. Walker, M. Shaikh, R. S. Defries, and J. Qi, "Derivation and evaluation of global 1-km fractional vegetation cover data for land modeling," *J. Appl. Meteorol.* **39**, pp. 826–839, 2000.